Title

Chromosome-specific telomere lengths and the minimal functional telomere revealed by nanopore sequencing

Journal

Genome Research, 32(4)

ISSN

1088-9051

Authors

Sholes, Samantha L

Karimian, Kayarash

Gershman, Ariel

et al.

Publication Date

2022-04-01

DOI

10.1101/gr.275868.121

Chromosome-specific telomere lengths and the minimal functional telomere revealed by nanopore sequencing

Samantha L. Sholes,[1,2] Kayarash Karimian,[1,2] Ariel Gershman,[1,2] Thomas J. Kelly,[3] Winston Timp,[1,4] and Carol W. Greider[1,5]

[1]*Department of Molecular Biology and Genetics, Johns Hopkins University School of Medicine, Baltimore, Maryland 21205, USA;* [2]*Biochemistry, Cellular and Molecular Biology Graduate Program, Johns Hopkins University School of Medicine, Baltimore, Maryland 21205, USA;* [3]*Program in Molecular Biology, Sloan Kettering Institute, Memorial Sloan Kettering Cancer Center, New York, New York 10065, USA;* [4]*Department of Biomedical Engineering, Johns Hopkins University School of Medicine, Baltimore, Maryland 21205, USA;* [5]*Department of Molecular Cell and Developmental Biology, University of California, Santa Cruz, California 95064, USA*

We developed a method to tag telomeres and measure telomere length by nanopore sequencing in the yeast *S. cerevisiae*. Nanopore allows long-read sequencing through the telomere, through the subtelomere, and into unique chromosomal sequence, enabling assignment of telomere length to a specific chromosome end. We observed chromosome end–specific telomere lengths that were stable over 120 cell divisions. These stable chromosome-specific telomere lengths may be explained by slow clonal variation or may represent a new biological mechanism that maintains equilibrium unique to each chromosome end. We examined the role of *RIF1* and *TEL1* in telomere length regulation and found that *TEL1* is epistatic to *RIF1* at most telomeres, consistent with the literature. However, at telomeres that lack subtelomeric Y′ sequences, *tel1Δ rif1Δ* double mutants had a very small, but significant, increase in telomere length compared with the *tel1Δ* single mutant, suggesting an influence of Y′ elements on telomere length regulation. We sequenced telomeres in a telomerase-null mutant (*est2Δ*) and found the minimal telomere length to be ∼75 bp. In these *est2Δ* mutants, there were apparent telomere recombination events at individual telomeres before the generation of survivors, and these events were significantly reduced in *est2Δ rad52Δ* double mutants. The rate of telomere shortening in the absence of telomerase was similar across all chromosome ends at ∼5 bp per generation. This new method gives quantitative, high-resolution telomere length measurement at each individual chromosome end and suggests possible new biological mechanisms regulating telomere length.

[Supplemental material is available for this article.]

Maintenance of the telomere length equilibrium is critical for cell survival. Telomeres shorten with each cell division, whereas a few are stochastically elongated by the enzyme telomerase (Greider and Blackburn 1985; Teixeira et al. 2004). This balance of shortening and lengthening is exquisitely regulated to generate a normal distribution of lengths that is established around a mean or "set point." Different species have very different telomere length set points; for example, *Oxytricha* has 20–30 bp, yeasts have 300 bp, humans have 10 kb, and some mouse strains have up to 80 kb mean telomere lengths (Greider 1996). How this distribution is established and maintained is not fully understood. When telomerase levels are low or absent, the distribution shifts toward shorter lengths, and the shortest telomeres signal a DNA damage response. These cells undergo a permanent cell cycle arrest, termed senescence or apoptosis, depending on the cell type (Enomoto et al. 2002; d'Adda di Fagagna et al. 2003; IJpma and Greider 2003).

Loss of telomere length maintenance in humans leads to disease. Individuals with inherited mutations in telomerase, or other telomere regulatory genes, have short telomere syndrome, which includes bone marrow failure, immunodeficiency, pulmonary fibrosis, and other diseases (Armanios 2013). In contrast, activation of telomerase (Counter et al. 1992; Greider 1998) or inheritance of long telomeres allows cell immortalization, which can predispose to cancer (Stanley and Armanios 2015; McNally et al. 2019). Thus, deviation from the mean telomere length in either direction affects cellular lifespan and plays a critical role in disease.

The yeast *Saccharomyces cerevisiae* serves as an excellent model for probing mechanisms of telomere length regulation. Many genes and regulatory mechanisms that affect human telomere length were first discovered in yeast (Wellinger and Zakian 2012). Yeast telomere sequences are more variable than the consistent TTAGGG repeats found in vertebrates (Moyzis et al. 1988). They are composed of a mixture of GT, GGT, or GGGT sequence motifs, usually abbreviated, $G_{1\text{-}3}T$. The subtelomeric region in yeast contains specific families of repeated DNA.

Deletion of any component of telomerase in yeast leads to progressive telomere shortening, termed ever-shorter telomere (EST) phenotype (Lundblad and Szostak 1989; Lendvay et al. 1996). Previous work suggests that telomeres shorten by ∼3–5 bp per cell division in the absence of telomerase and that this value is constant and independent of telomere length (Marcand et al. 1999; Wellinger and Zakian 2012; Xu et al. 2013). There is initially no effect of telomere shortening on cell growth and survival, but

Corresponding author: cgreider@ucsc.edu
Article published online before print. Article, supplemental material, and publication date are at https://www.genome.org/cgi/doi/10.1101/gr.275868.121.

32:616–628 Published by Cold Spring Harbor Laboratory Press; ISSN 1088-9051/22; www.genome.org

when telomeres become very short after passaging in culture for several days, most cells arrest at G_2/M (Enomoto et al. 2002; IJpma and Greider 2003). A few cells can rescue their short telomeres through recombination and will generate "survivors" that grow in the absence of telomerase (Lundblad and Blackburn 1993). Survivors are generated through a break-induced replication (BIR) pathway (Bosco and Haber 1998; McEachern and Haber 2006) that can initiate within the telomere repeats (Type II survivors) or in the subtelomere repeated elements (Type I survivors) (Teng and Zakian 1999). Deletion of the recombination gene *RAD52* significantly reduces production of both types of survivors (Lundblad and Blackburn 1993), although very rare survivors have been found in *est2Δ rad52Δ* double mutants (Lebel et al. 2009).

The normal distribution of the telomere length equilibrium is due primarily to sequence loss through replication and sequence addition by telomerase. Shampay and Blackburn (1988) showed that independent chromosome ends can slightly shift their mean length owing to clonal variability. If a cell that happens to have a short telomere at Chromosome 8L, for example, seeds a new colony on a plate, the descendants of that cell will initially have a new, shorter telomere length distribution until enough divisions occur in the population to homogenize all ends toward a population mean (Shampay and Blackburn 1988).

The "protein counting" model for telomere length regulation established in *S. cerevisiae* (Marcand et al. 1997, 1999) proposes that proteins bound to the telomeric repeats negatively regulate telomere elongation by telomerase, so that the probability of telomere elongation decreases with telomere length. Mean telomere length is stable when the average rate of length-dependent elongation is equal to the average rate of length-independent shortening. (Bianchi and Shore 2008). This model has received significant attention and is now the accepted model for telomere length regulation in organisms as distantly related as mammals, plants, and fission yeast (Smogorzewska and de Lange 2004; Watson and Riha 2010; Wellinger and Zakian 2012; Armstrong and Tomita 2017; Maciejowski and de Lange 2017). Sequence analysis of individual telomeres showed that telomerase added between 3 bp and 179 bp (average, 44 bp) onto chromosome ends in one cell cycle; however, only a few telomeres were elongated at each cycle. Further, shorter telomere repeat tracts were preferentially elongated compared with those with longer repeat tracts (Marcand et al. 1999; Teixeira et al. 2004). This work further supported the protein counting model by providing evidence that telomerase preferentially elongates short telomere repeat tracts. How preferential elongation of short telomeres allows the robust maintenance of the telomere length equilibrium over many cell divisions is not yet clear.

The standard technique for visualizing telomere length in yeast is by Southern blot. Genomic DNA from yeast cells is cut with a restriction enzyme near the telomere and hybridized with a probe to the telomere repeats or to the subtelomere, generating smeared bands visible on the autoradiogram (Shampay and Blackburn 1988). The smears represent the heterogenous distribution of telomere lengths across both the different chromosomes and between cells. Because restriction sites on different chromosomes are at different locations, the absolute size of each smear differs. Frequently, the restriction enzyme XhoI is used to cut genomic DNA because many telomeres have a conserved XhoI restriction site in the Y′ subtelomere element. Multiple telomeres are then visualized in a heterogeneous band centered at ~1.2 kb. Measuring median length of this 1.2-kb-sized band can allow large changes in bulk telomere length to be measured in various mutant backgrounds, but it is not possible to deconvolute the length of individual telomeres from each other.

To provide a more quantitative analysis of telomere length variation, we developed a nanopore sequencing method to measure telomere length. Nanopore sequencing allowed us to capture a full telomere sequence as well as the subtelomere and unique chromosomal sequence in one long read. Using this quantitative method for measuring telomere length, we re-evaluated fundamental questions about telomere length distribution and changes in mutant backgrounds that alter telomere length.

Results

Telomere tagging and bioinformatic analysis

To accurately measure telomere length and retain the telomeric 3′ overhangs, we modified a method (Teixeira et al. 2004) to tag the molecular end of the chromosome. We prepared high-molecular-weight (HMW) DNA (Denis et al. 2018) and added poly(A) to the 3′ ends with terminal transferase. We next annealed an oligo (dT) primer that also contained a unique adapter sequence, termed TeloTag. The addition of *Sulfolobus* DNA polymerase IV, which lacks strand displacement and exonuclease activity, was used to generate a double-stranded blunt end, as well as T4 DNA ligase to seal the nicks. Nanopore library adaptors were added to allow sequencing (Fig. 1A).

Tagged genomic DNA was run on nanopore MinION or Flongle flowcells to generate whole-genome sequencing (WGS) data (Fig. 1B). For optimal use of a nanopore MinION flowcell, samples were multiplexed, and only reads with barcodes on both ends were retained. Raw reads with telomeric sequence were extracted using TideHunter (Gao et al. 2019). To ensure that reads had sequenced to the end of the telomere, we retained reads only if they contained the TeloTag. Adapter sequences were then bioinformatically removed using Porechop to ensure that they are not calculated as part of the telomere length (https://github.com/rrwick/Porechop). These filters were used on the raw reads before alignment. The resulting reads were aligned using minimap2 to a *S. cerevisiae* reference genome, sacCer3 (Foury et al. 1998). To ensure that the reads mapped only to the correct chromosome end, we removed all reads that aligned in multiple places in the genome using SAMtools to select only reads with a map quality score greater than 20 and to remove all secondary and supplemental alignments. Finally, the position where the subtelomere ends and telomere repeats begins was identified for each chromosome end, and the telomere sequence length was calculated using the aligned reads (see Methods) (Fig. 1C).

Telomere length by nanopore sequencing recapitulates length measurement by Southern blot

To test the accuracy of our nanopore method for telomere length measurement, we compared telomere fragment length analysis by nanopore and Southern blot. We first looked at strains with expected clear differences in telomere length profiles, wild type and *rif1Δ*. Deletion of the *RIF1* gene results in very long telomeres on Southern blots (Hardy et al. 1992), allowing us to probe a greater distribution of telomere length profiles and test whether these length differences are captured with nanopore sequencing. We measured telomere fragment length after XhoI digest using a probe against the common Y′ subtelomere element; this will measure telomere lengths in bulk, probing 17 of 32 subtelomeres (Fig. 2A; Supplemental Fig. S1C). We ran all samples in duplicate on a Southern blot and included an additional probe to the unique sequence at CEN4 that runs at 1.4 kb as an internal molecular marker for densitometry plots (Fig. 2A; Supplemental Fig. S1C). We used

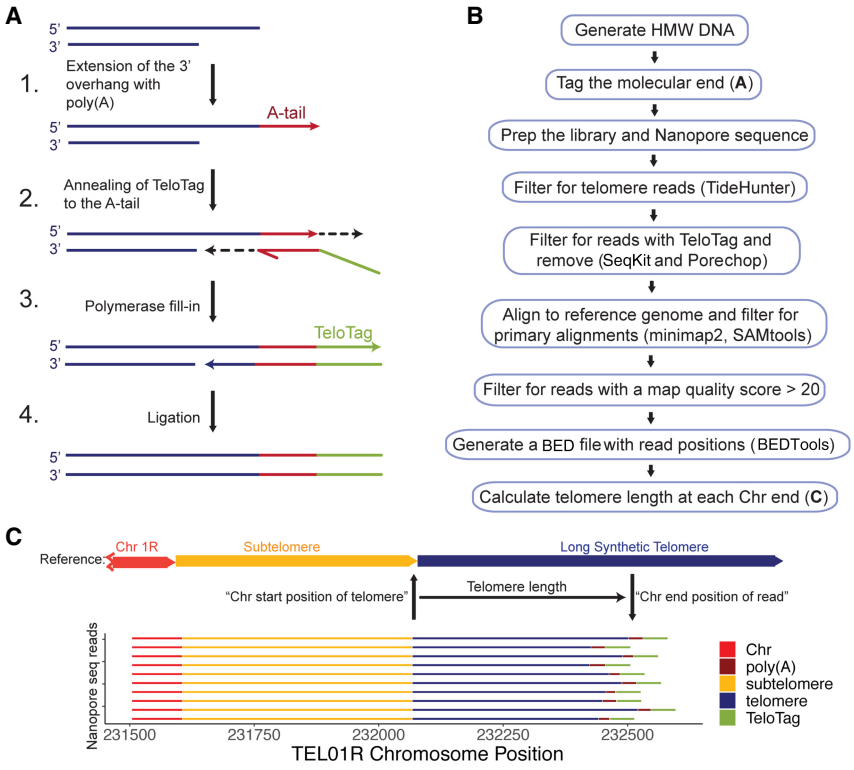

Figure 1. Telomere length measurement by nanopore sequencing. (*A*) Schematic of method to tag the molecular end of the chromosome. (*1*) Terminal transferase adds poly(A) sequence to the 3′ overhang of the telomere. (*2*) A complementary oligo(dT) sequence on the TeloTag oligonucleotide end containing a unique TeloTag sequence is annealed to the poly(A) sequence. (*3*) Polymerase fill-in generates double-stranded blunt ends. (*4*) Ligase is used to seal the nick. Nanopore adaptors are then added using the manufacturer's protocol. (*B*) Bioinformatic pipeline to generate telomere length information (see Methods). (*C*) Telomere length is calculated using the chromosomal position of each telomere sequence start and calculating the distance to the TeloTag sequence at the chromosome end. A random sample of 10 sequence reads aligned at TEL01R is presented as an example.

densitometry scanning to quantify the signal on the Southern blot (see Methods).

On the same samples, we performed our nanopore sequencing method as described (Methods) (Fig. 1). Nanopore sequencing data statistics are summarized in Supplemental Table S1. To directly compare to Southern blot telomere length, we included the internal chromosomal sequence up to the XhoI site for Y′ on the nanopore telomere read file. The histogram of the nanopore telomere sequence read lengths aligned well with the Southern blot densitometry for both wild-type telomeres and the much longer *rif1Δ* telomeres in two different strains (Fig. 2B; Supplemental Fig. S2A). The differences at the edges of the telomere length distribution between the nanopore and noisier Southern densitometry data highlight the increased ability to detect subpopulations in nanopore that are not detected by Southern blotting densitometry scans (Fig. 2D; Supplemental Fig. S2B). We used WALTER, a tool for Southern blot densitometry that generates summary length statistics (Lyčka et al. 2021), to compare Southern blot and nanopore telomere length profiles, and again saw comparable results (Supplemental Fig. S3A). We then generated Q–Q plots to examine the distribution of nanopore and Southern density data against a normal distribution (Supplemental Fig. S4A,B) and against each other (Supplemental Fig. S4C). The linearity of the Q–Q plots of both the Southern and nanopore data confirms that these profiles resemble a normal distribution (for details, see Supplemental Fig. S4), and we assumed a normal distribution for our statistical analysis throughout this work, including calculating correlation coefficients between data sets, performing *t*-tests, and performing analysis of the mean (ANOM) testing. The sample standard deviations of nanopore and Southern density distributions were similar, and there was no significant difference in the means by Welch's *t*-test (Supplemental Fig. S3A).

Because the Y′ probe measures 17 telomere length distributions simultaneously, it is challenging to detect potential small effects and chromosome-specific telomere lengths with this probe on a Southern blot. To assess the length distribution of single chromosome ends, we generated strains in which the subtelomere was replaced by a unique sequence. We used two different strains (Shubin et al. 2021) with unique sequence at either chromosome end TEL01L unique end 1 (strain UE1) or at chromosome end TEL11R unique end 11 (strain UE11) (Supplemental Fig. S1A,B). We examined the telomere lengths of these single TEL01L and TEL11R chromosome ends in both wild-type and *rif1Δ* backgrounds, using a probe to the unique ends (Fig. 2C; Supplemental Fig. S1D). Again, we saw good agreement between the single telomere length distributions determined by nanopore sequencing and Southern blotting (Fig. 2D; Supplemental Fig. 2B). In both genetic backgrounds, we observed no significant differences between the sample means (Supplemental Fig. S3B). We conclude that nanopore sequencing can accurately measure telomere fragment length in a bulk population or single telomere population across different telomere length profiles.

To determine the most effective flowcell type to achieve the minimum number of reads required for telomere length measurement using nanopore sequencing, we compared the MinION flowcells to the lower-cost, but lower-yield, Flongle flowcells. Multiplexing two samples per Flongle and MinION flowcell yielded many fewer reads from the Flongle (about 150–250 per barcode) versus the MinION (about 2000 reads per barcode), but we found no statistically significant differences between the mean and distributions of bulk telomere lengths across technical replicates and flowcell types (Supplemental Fig. S5). Thus, although the lower-cost Flongle flowcells yield reliable bulk telomere length data, the low number of reads does not allow analysis of individual chromosome ends (see below) and thus may not provide as useful a platform for investigating telomere biology.

Each chromosome end shows reproducible chromosome-specific telomere length distributions

Probing telomere lengths on unique chromosome ends is challenging with Southern blots, but nanopore sequence reads are long enough to span the subtelomeric elements and extend into

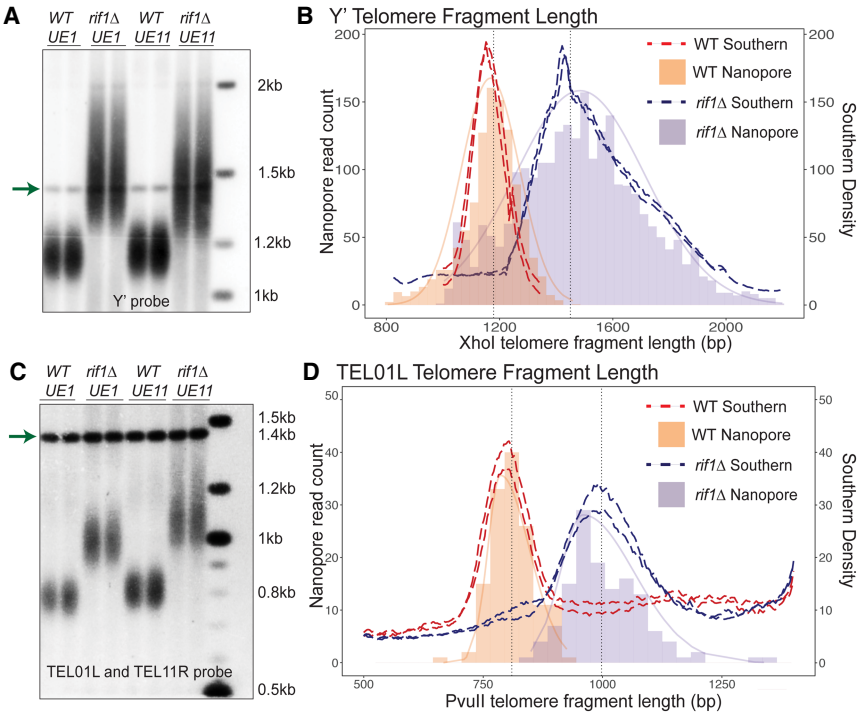

Figure 2. Telomere fragment length measured by nanopore sequencing accurately reflects length measurements by Southern blot. (*A*) Southern blot probed with Y′ subtelomeric probe and with CEN4 probe (arrow) as a marker at 1.4 kb to calibrate for densitometry. Two replicates of wild-type (WT) cells and two replicates of *rif1Δ* cells are shown for each strain, UE1 and UE11. (*B*) Comparison of densitometry (dotted lines) of Southern blot shown in *A* and nanopore sequencing (histogram fill bars) for UE1 strain. The light orange bars represent nanopore read counts for WT cells; the light purple bars represent nanopore read counts for *rif1Δ* cells. The spike in densitometry data at 1400 bp is owing to the CEN4 internal control signal. (*C*) Southern blot probed with the unique single telomere TEL01L probe and CEN4 probe (arrow). (*D*) Comparison of densitometry (dotted lines) of Southern blot in *C* and nanopore sequencing (bars) of UE1 TEL01L. The light orange bars represent nanopore read counts for WT cells; the light purple bars represent nanopore read counts for *rif1Δ* cells.

unique chromosomal sequence. To examine individual chromosome ends, we sequenced three independent wild-type clones and three *rif1Δ* clones (Supplemental Fig. S6B). For the wild type, we used two independent clones of UE1 and one clone of UE11. Each clone was isolated by picking an independent single colony from a freshly streaked plate of cells (Supplemental Fig. 6B). We analyzed both the bulk telomere length of all telomeres and individual chromosome ends (Fig. 3A).

We tested alignment to the S288C (Foury et al. 1998) as well as the W303 (Berlin et al. 2015; Matheson et al. 2017) reference genomes (Supplemental Fig. S7) and found the genome assembly in the subtelomeres was more complete for S288C and allowed reads to correctly map to more specific telomeres, so we used S288C as the reference. We were able to individually map 20 of 32 total chromosome ends with unique subtelomere and upstream genic sequences in our UE1 and UE11 strains. However, we were not able to map 12 chromosome ends uniquely (TEL01R, TEL02R, TEL03R, TEL06L, TEL07L, TEL09L, TEL12L, TEL12R, TEL13R, TEL14R, TEL16L, and TEL16R) owing to variation in subtelomeric structure from the reference genome. Subtelomeric elements are known to recombine and generate end diversity (Louis and Haber 1990, 1992; Maxwell et al. 2004), and we therefore excluded these 12 difficult to map telomeres in our analysis.

We were surprised to find that some chromosome ends showed telomere length distributions that were consistent across three independent clones but distinctly longer or shorter from the population mean of all telomeres (Fig. 3A). To quantify the differences, we applied ANOM (Pallmann and Hothorn 2016) to compare the mean length of individual chromosome ends to the population mean length of all the telomeres and found that eight chromosome ends (TEL04L, TEL04R, TEL08L, TEL10L, TEL11L, TEL11R, TEL13L, and TEL14L) had significantly shorter telomeres than the population mean, whereas six chromosome ends (TEL02L, TEL03L, TEL05L, TEL05R, TEL07R, and TEL09R) had significantly longer telomeres than the population mean (Supplemental Fig. S8A). A pairwise comparison of the three data sets suggests that telomere length of individual chromosome ends was consistent across replicates with correlation coefficients (r) of 0.96, 0.91, and 0.91 (Fig. 3B). We note that for chromosomes for which both ends could be analyzed, there was a trend toward concordance with both ends being long like TEL05L/5R and TEL015L/15R or with both ends being short like TEL04L/4R, TEL08L/8R, and TEL11L/11R, but there was no correlation between the length of chromosomes and the mean length of telomeres.

To determine whether chromosome end–specific lengths were maintained in the absence of Rif1, we analyzed two *rif1Δ* clones from UE1-1 and UE11 (Supplemental Fig. S6). Each clone showed telomeres whose mean lengths were significantly different from the clonal population mean (Supplemental Fig. S10A–C). However, in contrast to the wild-type cells, we did not see consistent length differences at individual chromosome ends in the two clones, evidenced by the correlation coefficient of 0.039 (Supplemental Fig. S10D). Because of the lack of correlation, we performed ANOM separately for the two clones and found significant deviations from the mean as expected from the broader length distribution seen in Figure 2 (Supplemental Fig. S10B,C). These results suggest that deletion of *RIF1* may disrupt the mechanism responsible for maintenance of telomere-specific lengths or that the very broad length distribution obscures the differences between specific telomeres.

The apparent chromosome end–specific telomere lengths in wild-type cells could be due to stochastic clonal variation as previously proposed (Shampay and Blackburn 1988). That is, when a cell with a short telomere on Chromosome 4L forms a new colony, it will seed a new telomere distribution that will center around a shorter midpoint (Fig. 3D). We found a few cases of statistically significant variation among the three clones analyzed. In particular, TEL03L was significantly shorter in UE11 than in UE1-1 and UE1-2, and TEL08R was significantly longer in UE1-1 than in UE1-2 and UE11, and TEL10R was significantly longer in UE1-1 and UE1-2 than in UE11 (Fig. 3C). This rate of clonal variation was infrequent compared with the rate of clonal variation

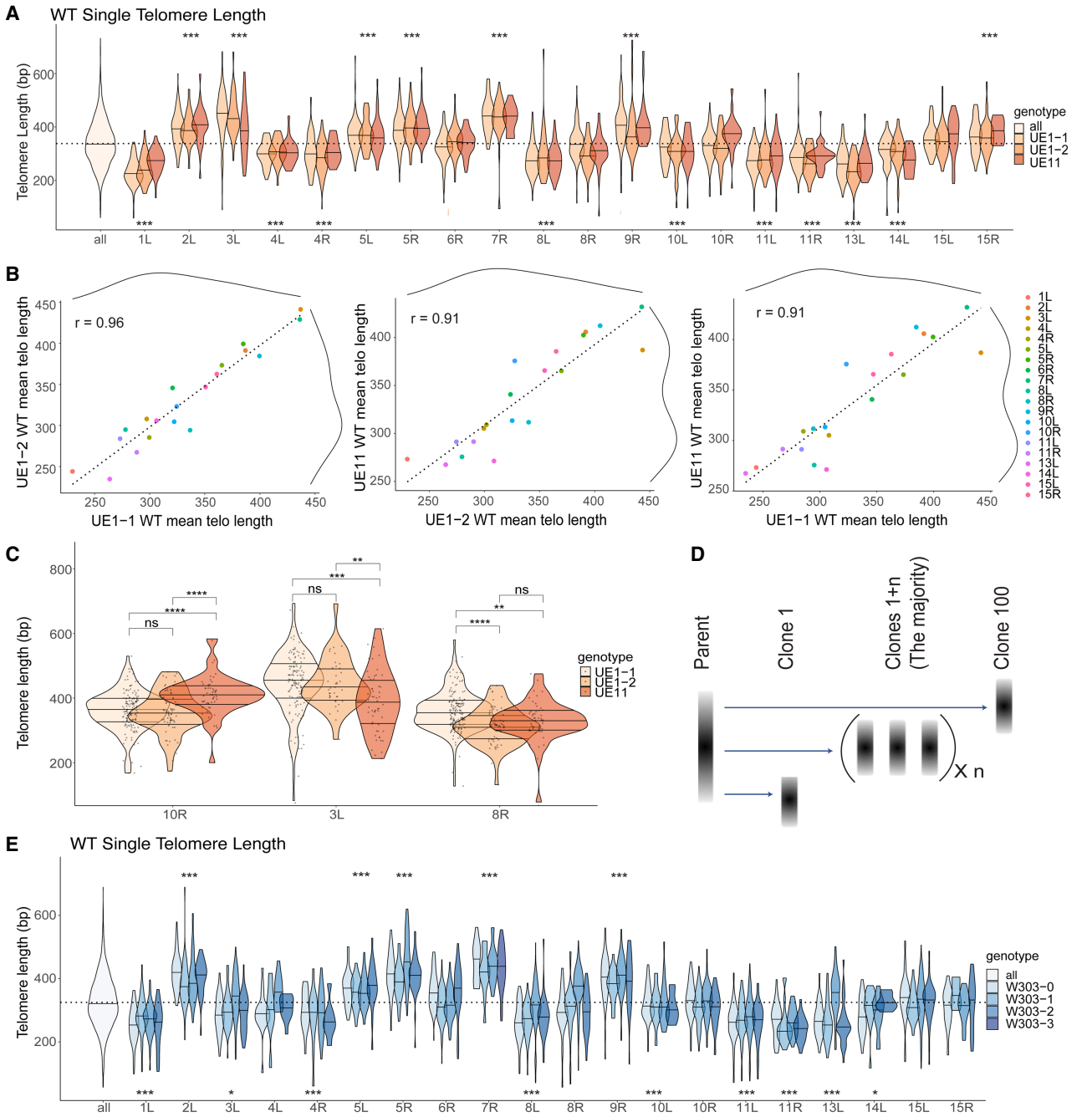

Figure 3. Nanopore sequencing mapping of the telomere length distribution of each individual chromosome end. (*A*) Bulk telomere length (all) and telomere length for each chromosome end were mapped by aligning to internal unique sequences. Three independent clones were sequenced: two from UE1 (UE1-1 and UE1-2) and one from UE11 (see Supplemental Fig. S6). Telomere lengths are reported as violin plots with a line at the mean. A dotted line shows the mean of the total population at 343.3 for WT cells. Analysis of the mean (ANOM) multiple contrast test of each telomere against the grand mean of all telomere length profiles was performed (see Supplemental Fig. S8A), and *P*-values adjusted by the Bonferroni method are reported as (*) <0.05, (**) <0.01, (***) <0.001, (****) <0.0001, or (n.s.) not significant. To note, TEL01L is engineered (as described in the text) in the UE1 strains, and TEL11R is engineered in the UE11 strains. (*B*) Pairwise correlations of mean telomere length across each of the three replicates for WT. A linear model was fit to the data (dotted line) to calculate the correlation constant, reported as the *r*-value. Marginal density of each data set is plotted as solid black lines across the *top* and *right* of the plots to show the spread of telomere lengths across each population. (*C*) Clonal variation was observed at TEL10R, TEL03L, and TEL08R in WT cells. Individual telomere length reads are represented as single points within the violin plots. The significance of the difference between two samples was tested using a multiple *t*-test (Methods) and *P*-values adjusted by the Bonferroni method are reported as above. (*D*) Model of clonal variation in which the telomere length of the majority of clones remains at the parental average, but occasional length outliers may seed new distributions represented by Clone 1 and Clone 100. (*E*) Three independent clones from the W303-0 parent were passages for 120 population doublings in independent cultures. The resulting clones W303-1, W303-2, and W303-3 were sequenced along with the parent W303-0 (see Supplemental Fig. S9A). Telomeres for each chromosome end were mapped by aligning to internal unique sequence. ANOM multiple contrast test of each telomere against the grand mean of all telomere length profiles was performed (see Supplemental Fig. S8B) and *P*-values adjusted by the Bonferroni method are reported as (*) <0.05, (**) <0.01, (***) <0.001, (****) <0.0001, or (n.s.) not significant.

in the previous study (Shampay and Blackburn 1988), although this may be due to different number of cell divisions in propagating clones.

Shampay and Blackburn (1988) introduced the concept of the telomere length "set point," in which all telomeres will gradually move back toward a population mean length distribution and suggested that differences in mean telomere length between clones might be erased during further propagation with all telomeres evolving toward a common mean length. Therefore, given enough cell divisions in the presence of telomerase, we might expect all chromosome ends to approach a mean value. In fact, Shampay and Blackburn (1988) showed that continued growth in liquid culture led to a broadening of the length distribution, which they interpreted as homogenization of all end lengths. The "protein counting model" for telomere length regulation (Marcand et al. 1997) suggests that telomere length is actively regulated around a mean based on the number of Rap1 proteins bound and, thus, the length of telomere sequence. These length regulation models are supported by the observation that telomerase apparently preferentially elongates short telomeres while ignoring long ones (Marcand et al. 1999; Teixeira et al. 2004). To test whether the telomere lengths would homogenize with more cell divisions, we isolated a clone of W303 cells (W303-0) and propagated it in liquid culture for 120 generations. Strain W303-0 is the parent of the clones UE1-1, UE1-2, and UE11 analyzed in Figure 3A (Supplemental Fig. S6A) and has a similar pattern of end-specific telomere lengths with some exceptions, such as that at TEL03L, which could be due to clonal variation. After 120 generations in liquid culture, three independent clones were isolated on plates and sequenced (W303-1, W303-2, and W303-3) (Supplemental Fig. S9A). We expected, based on previous models, that the telomere length distributions at individual chromosome ends would revert toward a grand population mean with more cell divisions. However, we saw that most chromosome-specific telomere lengths were maintained across all W303 clones, for example TEL02L, TEL04L, TEL04R, TEL05L, TEL05R, TEL 07R, TEL08L, TEL08R, TEL09R, TEL 10L, TEL10R, TEL11L, TEL11R, TEL1 3L, and TEL14L (Fig. 3E; Supplemental Fig. S8B). Although there were some examples of significant deviations from the initial length, for example, at TEL03L, TEL06R, TEL15L, and TEL15R, the major trend was reproducibility of the parents' chromosome end–specific lengths (Supplemental Fig. S8A,B). To quantify the variation between different clones, we examined pairwise correlations between the W303-0 parent and the W303-1, W303-2, and W303-3 subclones and found correlation coefficients (r) of 0.92, 0.82, 0.89, 0.82, 0.86, and 0.75 (Supplemental Fig. S9B). Our data indicate that after 120 doublings, the chromosome end–specific telomere lengths are largely maintained. This implies a very slow rate of reversion to a common mean length distribution, if it occurs at all, and implies new models for telomere length regulation are needed to explain these data.

Y′ elements have a small effect on telomere length regulation by *TEL1* and *RIF1*

The possibility of chromosome end–specific telomere lengths raised the idea that subtelomeric sequence might influence telomere length. A similar suggestion was made by Craven and Petes (1999), who proposed that the subtelomeric X and Y′ elements influenced the effects of *TEL1* and *RIF1* on telomere length. Specifically, they suggested that *TEL1* is epistatic to *RIF1* only at telomeres with Y′ elements but not at telomeres with only X elements. That is, telomeres are long in *rif1Δ* mutants, short in *tel1Δ* mutants, and also short in the *tel1Δ rif1Δ* double mutant at Y′ telomeres.

We reexamined this question using both Southern blots and nanopore sequencing. We generated *tel1Δ*, *rif1Δ*, and *tel1Δ rif1Δ* mutants in the in UE1 background (see Methods). As expected, in the Southern blot probed with Y′ sequence, *rif1Δ* mutants had long telomeres and *tel1Δ* mutants had short telomeres. The double mutant, *tel1Δ rif1Δ*, had short telomeres very similar to the single *tel1Δ* mutant (Fig. 4A), indicating that *TEL1* is epistatic to *RIF1* at telomeres with Y′ elements. Nanopore sequencing showed the same result at chromosomes with Y′ elements; *tel1Δ rif11Δ* double mutants had short telomeres indistinguishable from *tel1Δ* telomere lengths, supporting the previous finding (Fig. 4B). However, for chromosome ends that lacked Y′ elements and thus had only X elements, telomere length in *tel11Δ rif11Δ* was slightly longer (~65

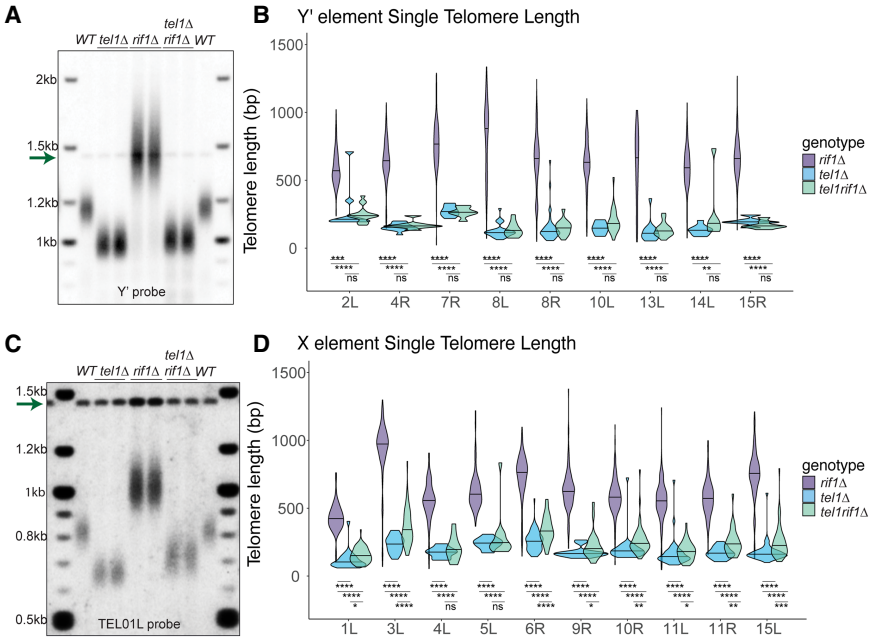

Figure 4. Y′ element subtelomeric sequences have a small effect on telomere length regulation by *TEL1* and *RIF1*. (*A*) Southern blot of WT, *tel1Δ*, *rif1Δ*, and *tel1Δ rif1Δ* cells with bulk telomere length hybridized with the Y′ and CEN4 probes (arrow). (*B*) Individual telomere lengths determined by nanopore for telomere ends containing Y′ subtelomeric elements reported for *tel1Δ*, *rif1Δ*, and *tel1Δ rif1Δ* cells. (*C*) Southern blot of WT, *tel1Δ*, *rif1Δ*, and *tel1Δ rif1Δ* samples hybridized with unique probe to TEL01L and CEN4 probe (arrow) to examine unique TEL01L with no subtelomeric elements. (*D*) Individual telomere lengths determined by nanopore for telomere ends containing only X subtelomeric elements or no telomeric elements (TEL01L) reported for *tel1Δ*, *rif1Δ*, and *tel1Δ rif1Δ* cells. A multiple *t*-test was used to assess the significance of telomere length differences between genotypes, and *P*-values are reported as (*) <0.05, (**) <0.01, (***) <0.001, (****) <0.0001, or (n.s.) not significant.

bp on average) and statistically different from *tel1Δ* (Fig. 4D). This trend also was seen at the unique chromosome TEL01L, where the subtelomeric sequence was removed entirely. Both nanopore sequencing (Fig. 4D, TEL01L) and Southern blot (Fig. 4C) showed that telomeres in the *tel1Δ rif1Δ* double mutant were longer than the *tel1Δ* alone. Although the difference in length was not as large as seen by Craven and Petes (1999), it is reproducible and suggests the need for further study.

Telomere shortening in the absence of telomerase reveals the minimal functional telomere

To examine the dynamics of telomere loss in cells without telomerase, we examined telomerase-null cells. We sporulated an *EST2/est2Δ RAD52/rad52Δ* heterozygous diploid and selected individual haploid colonies of *est2Δ*, *est2Δ rad52Δ*, and wild type (*EST2*). We grew these genotypes from a single colony and passaged each three times in liquid culture (Supplemental Fig. S11). To determine population doubling numbers, we estimated growth from a single cell to colony formation to be about 20 cell doublings. Both *est2Δ* and *est2Δ rad52Δ* cells grew slowly after 55 population doublings, and *est2Δ rad52Δ* cells showed significantly slower growth than *est2Δ*. Telomere shortening in the absence of telomerase leads to cell cycle arrest (Enomoto et al. 2002; IJpma and Greider 2003), as well as to telomeric elongation by BIR (Bosco and Haber 1998) that ultimately allows the outgrowth of "survivors" (Lundblad and Blackburn 1993). This implies there must be a competition between arrest and BIR, and presumably, all chromosomes must be elongated for phenotypic survivors to emerge.

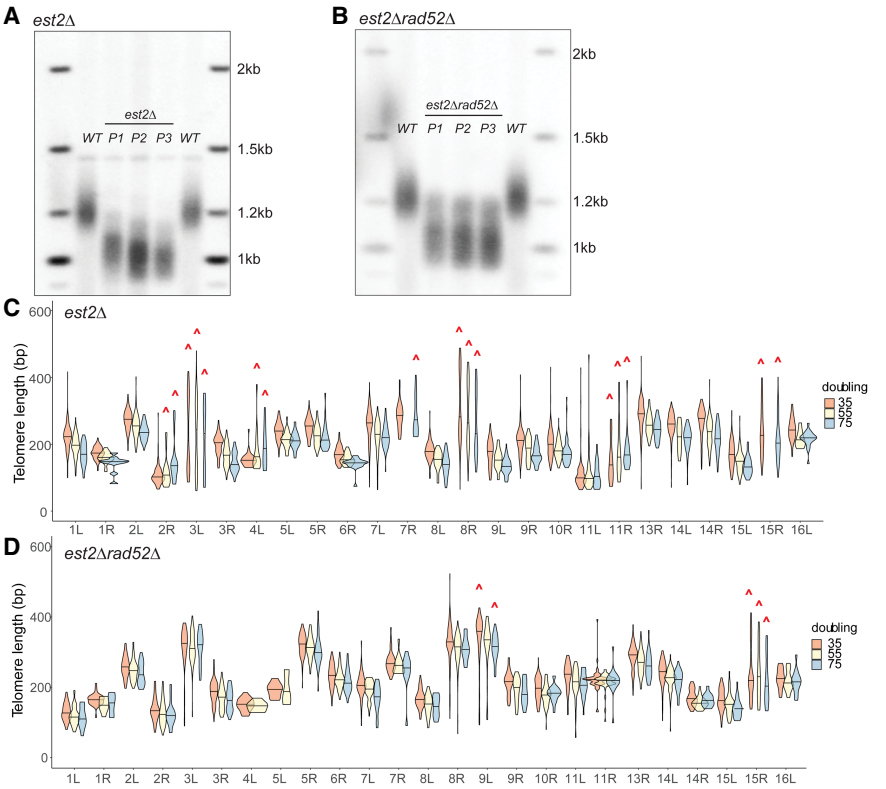

Figure 5. Telomere shortening and outlier elongation events in a telomerase-null, *est2Δ* background at individual telomeres over time. Freshly generated *est2Δ* and *est2Δ rad52Δ* haploids were grown up (P1, 35 doublings) and passaged twice (P2, 55 doublings; P3, 75 doublings) to allow for telomere shortening (see Methods). Telomere length was measured by Southern blot hybridized with the Y′ probe and by nanopore sequencing on the same samples. (*A*) Southern blot of WT, P1, P2, and P3 *est2Δ* hybridized with the Y′ probe. (*B*) Southern blot of WT, P1, P2, and P3 *est2Δ rad52Δ* hybridized with the Y′ probe. (*C*,*D*) Individual telomere length of *est2Δ* (*C*) and *est2Δ rad52Δ* (*D*) cells determined by nanopore sequencing of P1, P2, and P3. We calculated the sample standard deviations of (σ) of each telomere at every passage and in the wild-type parental strain. Telomeres for which the standard deviation was greater than that of the wild type are considered outliers and are marked with a red caret. At P2, 55 doublings, in the *est2Δ* sample, not enough data were collected at TEL07R and TEL15R to plot, and at P3, 75 doublings, in the *est2Δ rad52Δ* sample, not enough data were collected at TEL04L and TEL05L to plot.

The ability to measure the length distributions of individual telomeres using nanopore sequencing suggested that it might be possible to detect possible BIR events in the progeny of the *est2Δ* cells. Such events would not be visible by traditional Southern blotting of telomeres in bulk (Fig. 5A,B). In fact, we observed some telomere length distributions that were highly skewed, unlike any in the wild-type populations that we studied (see, e.g., TEL03L and TEL08R in Fig. 5C). To quantify this effect, we calculated the sample standard deviation of each telomere distribution in wild-type cells (P0; see Methods) and in *est2Δ* cells. For most telomeres we observed, as expected, that the sample standard deviation decreased relative to that of the parental wild-type telomere during passaging of the *est2Δ* cells. This observation is consistent with the fact that in the absence of Est2, telomeres progressively shorten, but their lengths are bounded by the minimum telomere length consistent with cell survival (see below). We found seven telomeres for which the sample standard deviation actually increased relative to that of the wild-type parent: TEL02R, TEL03L, TEL04L, TEL07R, TEL08R, TEL11R, and TEL15R (Fig. 5C). These telomere samples contain subpopulations with unexpectedly long telomeres, which we refer to below as outliers. Qualitative inspection of the distributions confirmed that these telomere distributions are highly skewed (Fig. 5C). Although we did not passage *est2Δ* cells for enough generations to observe outgrowth of survivors, our data suggest that telomere elongation events due to BIR may be occurring in these cells at an early stage, albeit at a relatively low frequency.

To further examine the role of BIR in the generation of outlier telomere lengths, we examined the *est2Δ rad52Δ* cells, which are recombination deficient (Fig. 5B/D). If the long telomere outliers in *est2Δ* cells are owing to BIR, we would expect to see fewer of these outlier length increases in *est2Δ rad52Δ* cells. Indeed, there was a trend toward fewer outliers as we saw only five examples of outlier telomeres at TEL09L and TEL15R in the *est2Δ rad52Δ* cells (Fig. 5D). These length increases may be owing to rare events that occur even in *est2Δ rad52Δ* cells that allow telomere elongation (Lebel et al. 2009; Claussin and Chang 2016). Nanopore sequencing will allow detailed mechanistic insight into telomere elongation by BIR and the generation of survivors.

To determine the rate of telomere shortening in the absence of telomerase before cell division arrest, we compared the rate of shortening at individual chromosome ends in *est2Δ* and *est2Δ rad52Δ* cells over three outgrowths or passages (P1, P2, P3) (Supplemental Fig. S11). We exclude data where the telomere length increases likely owing to BIR over the 75 population doublings at TEL02R and TEL11L in *est2Δ* cells, as it would skew the analysis. To establish the initial rate of shortening, we need to establish the initial telomere length before *EST2* deletion. Because this was not possible in the newly dissected haploid *est2Δ* strain, we instead used the wild-type telomere length for each chromosome as a proxy for the initial length and designated this P0 (Supplemental Fig. S11). The rate of shortening for each chromosome end was very similar from P0 to P1; there was a loss of 5.33 bp/population doubling in *est2Δ* and 5.13 bp/population doubling in *est2Δ rad52Δ* cells (Fig. 6A,B). This telomere shortening rate is similar to other estimates of 3-4 bp/population doubling (Marcand et al. 1999; Wellinger and Zakian 2012; Xu et al. 2013). If we include the later passages P2 and P3 in the rate, there is a continuous decline in the apparent rate because cells with very short telomeres do not divide and thus are lost from the calculated rate. To compare individual ends, we separately examined the rate of shortening from P1 to P3 and found all ends had a similar loss rate of 0.76 bp/population doubling in *est2Δ* cells and 0.39 bp/population doubling in *est2Δ rad52Δ* cells (Fig. 6A,B). The loss rates of the P1 to P3 *est2Δ* cells were higher than those of *est2Δ rad52Δ* cells on average perhaps owing to the more severe growth defects we observed in *est2Δ rad52Δ* compared with *est2Δ* cells. The rates of telomere shortening at each individual chromosome end were very similar in both *est2Δ* and *est2Δ rad52Δ*. Our quantitative single telomere data support previous analysis (Marcand et al. 1999) that telomere shortening rates are similar across chromosome ends.

To determine the minimum telomere length in telomerase-null cells, we examined telomeres at early passages before survivor events were predicted to occur (Lundblad and Blackburn 1993). We calculated the bottom 99th length percentile at each chromosome end and identified critically short telomeres in both the *est2Δ* and *est2Δ rad52Δ* ranging from 70 to 80 bp. The shortest three values are highlighted in each genotype at each passage (Table 1). This minimal telomere length is also consistent with the minimal length we found in telomerase-positive wild-type and *tel1Δ* cells of ~75 bp (Table 1). Previous work has suggested that telomeres <100 bp could be considered "critically short" (Abdallah et al. 2009). Our sequence analysis now more precisely identified a minimum of ~75 bp at individual chromosome ends.

Discussion

Nanopore telomere sequencing uncovered the unexpected finding of chromosome end–specific telomere length differences that were preserved across multiple independent clones over 120 population doublings. The stable maintenance of telomere-specific length differences, with mean values differing by as much as 200 bp, implies that current models for telomere length homeostasis require some revision (Marcand et al. 1997, 1999; Teixeira et al. 2004; Greider 2016). Both the protein counting and the replication fork models suggest that the average rate of telomere elongation by telomerase decreases with telomere length because of increased binding of inhibitory proteins to the telomeric repeats. In the context of this model, our new data indicate that the functional relationship between the number of bound proteins and the decrease in the average elongation rate is different for different telomeres. Thus, the balance point between length-dependent elongation and length-independent shortening occurs at different lengths for different telomeres. This finding implies the existence of as-yet-undiscovered telomere-specific influences on length homeostasis. It also suggests that the observed preferential elongation of short telomeres (Marcand et al. 1999; Teixeira et al. 2004) must be applied in a telomeric-specific sense, that is, preferential elongation of telomeres that are short relative to their specific equilibrium length. In addition, our new data indicate that the rate of shortening in the absence of telomerase is similar for all telomeres, confirming and extending previous studies (Marcand et al. 1999; Wellinger and Zakian 2012; Xu et al. 2013). It will be of interest to determine whether in the absence of telomerase, telomeres with a shorter equilibrium length may have a higher probability of becoming critically short and triggering cell cycle arrest.

Our work adds to other evidence showing that counting Rap1 binding proteins does not fully explain telomere length regulation. Alteration of the telomerase RNA template to generate TTAGGG repeats that do not bind Rap1 has little effect on telomere length (Henning et al. 1998; Alexander and Zakian 2003; Brevet et al. 2003; Bah et al. 2011). In addition, recent work suggests the apparent preferential elongation of short telomeres may be due to replication fork collapse in telomere

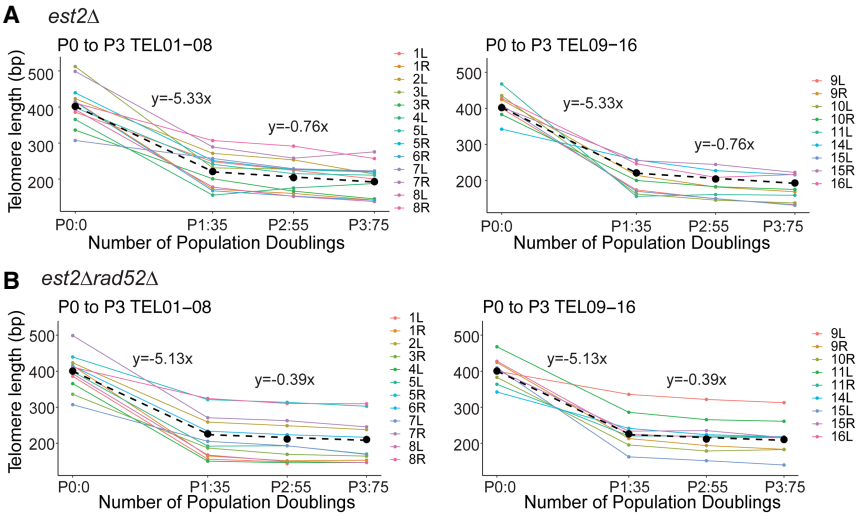

Figure 6. Telomere shortening rate in the absence of telomerase. (*A*) The progression of mean telomere length at individual chromosome ends in *est2Δ* cells over three passages. TEL01-08 and TEL09-16 are shown on separate graphs for clarity. The initial telomere length, P0, is estimated from the wild-type parental strain for each chromosome, and so it is not the exact genotype (see Results). The line of best fit to the average of the shortening rate is shown as a black dotted line. The rate of shortening for P0 to P1 and P1 to P3 are plotted separately because the two rates differ and each rate is reported *above* the line. (*B*) The rate of telomere shortening for the *est2Δ rad52Δ* strain was measured as described above in *A*.

Table 1. The bottom 99th percentile of telomere length

WT		*est2Δ P1*		*est2Δ P2*		*est2Δ P3*	
13L	77.25	10L	93.2	10L	79	10L	77.4
7R	96.06	11L	70.4	11L	71.6	11L	69.4
8R	96.19	2R	72	2R	75.6	8L	85
tel1Δ		***est2rad52Δ P1***		***est2rad52Δ P2***		***est2rad52Δ P3***	
13L	69.3	10L	86.45	10L	90.4	10L	76.75
4R	73.4	1L	89.6	1L	81.7	1L	71.9
8R	69.4	3L	171	2R	85	2R	71.95

The bottom 99th percentile of telomere length at the three shortest chromosome ends per genotype at each passage in *est2Δ*, *est2Δ rad52Δ*, as well as for wild type and *tel1Δ*. Minimum telomere length is ~75 bp.

repeats with subsequent elongation by telomerase (Paschini et al. 2020). Current models of length regulation need to be modified to account for end-specific equilibrium distributions and for Rap1-independent length maintenance.

What mechanism might regulate these end-specific telomere lengths? One obvious hypothesis is that sequences adjacent to the telomere repeats might affect length regulation, through either the sequence itself, chromatin modifications or transcription, or the noncoding RNA *TERRA* (Feuerhahn et al. 2010). In fact, there were small differences in response to *RIF1* length regulation at chromosomes that had Y′ elements compared with those that did not (Fig. 4). Subtelomeric DNA-binding proteins such as Tbf1 and Reb1 that have binding sites in X and Y′ are thought to play some role in length regulation (Berthiau et al. 2006). However, the small effect of these proteins cannot explain the large length differences of up to 200 bp on different chromosome ends observed in wild-type cells. The hint that there may be concordance between telomeres on the same chromosome (Fig. 3A,D) suggests that perhaps chromosome territories within the nucleus (Noma 2017) have an effect on length regulation. Alternatively, topologically associated domains (TADs) (Noma 2017) or localization to the nuclear periphery (Sobecki et al. 2018) may play a role in chromosome end–specific telomere length differences. The fact that deletion of *RIF1* disrupted telomere-specific lengths might provide a hint at the mechanism; however, it might be that that deletion of *RIF1* simply broadens the length distribution, obscuring any differences between telomeres. Nanopore sequencing of telomeres provides a method to further interrogate these interesting new questions.

In the absence of telomerase, all telomeres shortened at a similar rate as predicted by the end replication problem. A shortening rate of ~5 bp/population doubling is similar to what has been seen previously with other methods (Marcand et al. 1999; Abdallah et al. 2009; Wellinger and Zakian 2012; Xu et al. 2013). The shortest telomeres in telomerase-null cells, as well as in wild-type and *tel1Δ* cells, were ~75 bp. This is shorter than previously suggested (Abdallah et al. 2009) and allows specific hypotheses to be made for what might cause loss of telomere function. For instance, Rap1 binds telomeric DNA approximately every 20 bp (Gilson et al. 1993; Wahlin and Cohn 2000), so telomere dysfunction might be owing to loss of Rap1 binding or perhaps loss of the terminal nucleosome binding. However, it was observed previously that a yeast chromosome with human telomere repeats can be elongated by telomerase, even though Rap1 cannot bind human telomere repeats (Henning et al. 1998; Alexander and Zakian 2003; Brevet et al. 2003). This suggests that there may be distinct factors, independent of Rap1, that negatively regulate telomere length. We note that even at a minimal length of 75 bp, Ku should be able to bind DNA through its end binding function (Gravel et al. 1998; Chen et al. 2018). Given these new data on end-specific telomere lengths, it will be of interest to re-evaluate the role of specific protein binding in determining length regulation.

This novel nanopore sequencing method allows for the analysis of single molecules and provides the ability to assign telomere length measurement to individual chromosome ends. Leveraging this, we were able to uncover new aspects of telomere biology. Nanopore sequencing can be performed in any laboratory and requires relatively little capital investment. Even a smaller, less expensive Flongle flowcell provides a suitable number of independent reads for bulk telomere length measurement. With further improvements and the use of targeted enrichment (Gilpatrick et al. 2020; Kovaka et al. 2021), the cost and yield of this method can be even further improved. Telomere length measurement by nanopore sequencing will allow the telomere field to study new questions and revisit past unanswered questions in telomere biology. A different method of long-read sequencing, Pacific Biosciences (PacBio) sequencing, has recently been applied to human telomere sequences, (Grigorev et al. 2021) indicating long-read sequencing technologies are widely useful in telomere research. It will be of interest to determine whether chromosome end–specific telomere length differences are generalizable to other organisms, as well as perhaps even humans, and understanding how they are established and maintained will be a fascinating new area of telomere biology to explore.

Methods

Biological resources

Yeast strains and plasmid vectors used in this study are listed in Supplemental Tables S4 and S6. Yeast strains are available upon request and plasmid vector (pCS105) is available from Addgene (plasmid 174830).

Molecular cloning

Yeast molecular cloning, culturing, sporulation, and transformation were performed as previously described (Green and Sambrook 2012; Keener et al. 2019; Shubin et al. 2021).

The UE1 (previous named 1L 5×UAS landing pad) and UE11 (previously named 11R 5×UAS landing pad) constructs were designed in silico using SnapGene software and constructed as previously described (Shubin et al. 2021). UE11 was generated in the same manner as UE1, but with homology at chromosome arm 11R, rather than chromosome arm 1L. The subtelomere was removed in these strains using homology with the unique gene

region directly upstream of the telomere providing a 3′ overhang that is endogenously elongated by telomerase.

Yeast strain culturing and transformation

CVy61 (W303-0 WT haploids), UE1 (previously CALy117, *1L::leu2*), UE11 (previously CALy119, *11R::leu2*), UE1 *rif1Δ* (previously CALy202, *1L::leu2, rif1Δ::kanMX*), UE11 *rif1Δ* (previously CALy204, *11R::leu2, rif1Δ::kanMX*), and UE1 *tel1Δ* (previously CALy472, *1L::leu2, tel1Δ:: hphMX4*) strains were generated as previously described (Shubin et al. 2021). These strains were renamed UE1 and UE11 to highlight the function of a unique end, rather than a 5×UAS landing pad, which was important to this study. A list of all yeast strains and genotypes is presented in Supplemental Table S4.

The UE1 *tel1Δrif1Δ* was generated by transformation. Briefly, transformation was performed by treating 50 mL of logarithmically growing UE1 *rif1Δ* cells with 0.1 M lithium acetate (Sigma-Aldrich L6883) and adding 1 µg of linear DNA to replace *TEL1* with *tel1Δ::hphMX4* cassette for one-step integration. Cells were incubated for 10 min at 30°C before the addition of 0.5 mL 40% polyethylene glycol (PEG4000; Sigma-Aldrich P4338), 0.1 M lithium acetate. Cells were then incubated for 30 min at 30°C followed by a 45-min heat shock at 42°C. Cells were plated after a water wash onto YPD + Hygromycin B (Corning; at 200 µg/mL). Integration at the *TEL1* locus was confirmed by junction polymerase chain reaction (PCR). A list of primers and plasmids used in this study is presented in Supplemental Tables S5 and S6, respectively.

To perform the W303-0,1,2,3 experiment, CVy61 was streaked to single colony on YPD media. One colony was selected (W303-0) and grown in 5 mL YPD to 0.5 OD. This culture was split into two subcultures: (1) growth to 1.0 OD in 100 mL YPD broth for HMW genomic DNA extraction (see below) and called W303-0 for nanopore sequencing and (2) growth in 10 mL YPD broth to saturation for 24 h and passaged as 5 µL of saturated culture in 10 mL fresh YPD. This was repeated a total of five times before cells were plated onto YPD media. Three independent colonies were selected (W303-1, W303-2, and W303-3) to inoculate three cultures of 100 mL YPD broth for DNA extraction as described for subculture 1. We estimate 120 population doublings between W303-0 and W303-1,2,3 (for illustration, see Supplemental Figure S6A).

To perform the UE1 and UE11 experiments in wild-type and *rif1Δ* backgrounds, frozen stocks of UE1 wild type, UE11 wild type, UE1 *rif1Δ*, and UE11 *rif1Δ* were streaked onto YPD media to single colony. One colony each was selected from UE1 wild type, UE11 wild type, UE1 *rif1Δ*, and UE11 *rif1Δ*, grown to 0.5 OD in 5 mL YPD broth, followed by growth to 1 OD in 100 mL YPD for DNA extraction and nanopore sequencing as described above. An additional colony was selected from UE1 wild type and UE1 *rif1Δ* and grown in 10 mL YPD to saturation for 24 h and passaged as 5 µL of saturated culture in 10 mL fresh YPD. This was repeated a total of three times in liquid culture before cells were grown to 0.5 OD in 5 mL YPD broth and then to 1.0 OD in 100 mL YPD broth for DNA extraction and sequencing of UE1-2 wild type and *rif1Δ*. We estimate 60 population doublings between UE1-1 and UE1-2 (for illustration, see Supplemental Figure S6B).

To generate telomerase-null *est2Δ* and *est2Δ rad52Δ* cells, the heterozygous diploid strain yAY139 (IJpma and Greider 2003) was sporulated and dissected to yield sister spores for analysis.

Because these mutants will senesce with passaging, we attempted to keep cell division to a minimum, allowing telomeres to shorten but not form survivors (Chen et al. 2001). For both *est2Δ* and *est2Δ rad52Δ*, cells were taken directly from the original dissection plate and grown to saturation in 10 mL cultures of YPD broth. These mutant cultures were (1) grown to 1 OD in 100 mL for DNA extraction and sequencing, called passage 1 (P1) or (2) diluted to 10^5 cells/mL in YPD broth every 24 h before being grown to 1 OD in 100 mL for DNA extraction and sequencing. Dilution and growth for these mutants were continued for two more rounds, collecting cells after each passage called P2 and P3 (for illustration, see Supplemental Figure S10). A wild-type haploid spore was also selected from the original dissection plate of yAY139, grown to saturation in 10 mL YPD, and then grown to 1 OD in 100 mL YPD for DNA extraction and sequencing. This sample was called passage 0 (P0). The sample standard deviation of the telomeres in the P0 wild-type sample was compared with the telomerase-null telomere sample standard deviations as a threshold for characterizing potential recombinant telomere length outliers in the mutants. We additionally confirmed this outlier measurement with a qualitative examination of comparisons of mutant and wild-type telomere length distributions. This P0 wild-type sample was used a 0-population doubling initial length in examining the rate of telomere shortening.

HMW genomic DNA extraction

We modified a DNA isolation protocol (Denis et al. 2018) to collect HMW genomic DNA from yeast. Cultures were grown at 30°C to 1.0 OD in 100 mL YPD broth, collected in a Sorvall Legend XTR centrifuge with swinging bucket rotor for 5 min at 1500*g* and washed once with 20 mL TE buffer (10 mM Tris, 1 mM EDTA at pH 8.0).

To generate spheroplasts, cell pellets in a 50-mL conical centrifuge tube (Falcon) were resuspended in 2 mL 1 M sorbitol with 0.5 mL of 2.5 mg/mL zymolyase 100T (Amsbio 120493-1) and shaken gently (75 rpm) for 1 h at 30°C. Spheroplasts were collected at 300*g* for 4 min in the swinging bucket centrifuge, and the supernatant was carefully discarded.

Pelleted spheroplasts were lysed by resuspension in 1.7 mL lysis buffer (100 mM Tris at pH 7.5, 100 mM EDTA at pH 8.0, 500 mM NaCl, 1% PVP40) and 250 µL 10% SDS. After inverting the tube gently10 times, 20 µL of 100 mg/mL RNase A (Sigma-Aldrich R6513) was added, and the mixture was shaken at 75 rpm for 30 min at 37°C. To digest protein, 25 µL of 20 mg/mL Proteinase K (Invitrogen 25530-015) was added, and the mixture was incubated for 2 h at 50°C with occasional inversion until there was a uniform cloudy suspension.

To precipitate and remove protein, 5 mL TE and 2.5 mL 5M potassium acetate (pH 7.5) were added to the suspension, and the tube was inverted 10 times to mix and then placed on ice for 5 min. The tube was inverted again and placed on ice for an additional 5 min before centrifugation for 15 min at 4°C and 4000*g* in the swinging bucket centrifuge. The supernatant was decanted into a clean tube, and the centrifugation was repeated. The supernatant was again decanted into a clean tube.

DNA was precipitated by adding an equal volume of 100% isopropanol and swirling the tube until the DNA strands were observed. Precipitated DNA was collected from the bottom of the tube using a p1000 wide-bore pipette tip and placed in a clean Eppendorf microcentrifuge tube. The DNA was pelleted in a minicentrifuge for 15 sec and the supernatant carefully decanted. Then 500 µL 75% ethanol was added to rinse the DNA pellet. After decanting the wash, the residual ethanol was removed with a pipette tip. The DNA pellet was resuspended in 50–200 µL of EB buffer (Qiagen; 10 mM Tris-Cl at pH 8.5), depending on the size of the pellet. The DNA was allowed to resuspend on an inverting rotator overnight at 4°C. The final concentration of resuspended DNA was measured on a Qubit 3.0 fluorometer (Thermo Fisher Scientific).

DNA molecular end tagging

To tag the molecular end, HMW genomic DNA (gDNA, see above) was first A-tailed using terminal transferase (NEB M0315) in a reaction by incubating 2 µg of gDNA, 1× terminal transferase buffer, 1× $CoCl_2$, 5 mM dATP, and 20 U of terminal transferase enzyme for 1 h at 37°C, followed by heating for 10 min at 70°C to stop the reaction.

Five primers were designed to make a mixture of TeloTags (see Supplemental Table S6).

To the A-tailed gDNA reaction, the following were added to complete the TeloTag addition: 1× ThermoPol reaction buffer pack (NEB B9004S), 2.5 mM dNTP mix, 1 mM ATP, 2.5 mM TeloTag primer mix, and 4 U *Sulfolobus* DNA Polymerase IV(NEB M0327S). The TeloTag reaction was incubated in a Veriti 96-well thermal cycler (Applied Biosystems) for 1 min at 56°C and 10 min at 72°C. Four hundred units of T4 ligase (NEB M0202) was then added to the reaction and allowed to continue incubating for 20 min at 12°C. Ampere XP beads (Beckman Coulter) were used to purify the tagged gDNA from the reaction mixture.

Size selection of the tagged gDNA was performed using the short-read eliminator XS kit (Circulomics SS-100-121-01), which retains DNA molecules >10 kb. Once this step is completed, the tagged gDNA is ready for nanopore library preparation (see below).

Southern blotting and densitometry

HMW genomic DNA was extracted and quantitated as described above. Telomere length analysis by Southern blot was performed on the same strains used for nanopore sequencing according to a protocol previously described (Kaizer et al. 2015). Briefly, 250 ng of gDNA was digested with PvuII and XhoI for 2–4 h at 37°C and resolved on a 1% agarose gel overnight. Two concentrations of two-log ladders (NEB) were included as reference for analysis, 10 ng for single telomere assays and for bulk telomere assays. After transfer, the membrane was hybridized with ^{32}P-radiolabeled two-log ladder and PCR fragments unique to either TEL01L, TEL11R (a purified PCR product of the LEU2 gene and CYC1 terminator as described by Shubin et al. 2021), Y′ subtelomeric elements described by Kaizer et al. (2015), or CEN4 (Laterreur et al. 2018). After washing, the membrane was exposed on a storage phosphor screen (GE Healthcare) for 1 d for bulk assays and 4–5 d for single telomere assays. Southern images were captured on a STORM using ImageQuant (GE Healthcare). ImageQuant GEL files were downloaded into Adobe PhotoShop CS6 and saved as TIF files.

Southern blot densitometry was measured to allow for comparison to nanopore data as it shows both the normal distribution and spread of telomere length for each sample. However, these plots are often inconsistent and are not a direct measure of telomere length as they are generated from the Southern blot image. To somewhat counter this, we measured densitometry using two programs. We first used ImageQuant to generate a distribution fully across each sample lane to be overlaid with nanopore telomere fragment length data, so that all molecular markers and the resolution cut-off would be visible (Fig. 2C,D, F,G). In ImageQuant, we used the two-log ladder and the CEN4 band at 1.4 kb as molecular markers to determine a linear range, and the resulting CSV files were loaded into RStudio to generate telomere length plots. Second, PhotoShop TIF files were inverted and loaded into the WALTER ScanToItensity and IntensityAnalyzer to remove background and generate intensity profiles of the telomere signal alone (Lyčka et al. 2021). The reported summary statistics were loaded into RStudio to produce boxplots of telomere length.

Nanopore library preparation and sequencing

Library preparation of 1 µg input DNA with a molecular tag was performed using the native barcoding genomic DNA kit (Oxford Nanopore Technologies EXP-NBD104 and SQK-LSK109). Samples were run on a MinION flowcell (v.9.4.1) or Flongle flowcell (v.9.4.1 pore) using the MK1B or GridION for 24–72 h and were operated using MinKNOW software (v.19.2.2). Only reads with barcodes on both ends were selected to pass. The read counts and characteristics are shown in Supplemental Tables S1, S2, and S3. We note that this WGS sequencing from a MinION flowcell provides enough coverage (about 50–200 reads per telomere) to analyze specific single chromosome ends, but Flongle flowcells produce only about 10 reads at a single chromosome end, which, at present, are not enough to analyze specific single chromosome ends. On average, we found that a Flongle flowcell costs $33 per 100 telomere reads and 35 cents per 100 total reads (including flowcell and reagent costs), whereas a MinION flowcell costs $6.9 per 100 telomere reads and 4 cents per 100 total reads. We conclude that it may be more efficient to highly multiplex samples on a MinION flowcell to generate bulk telomere data than to use a Flongle flowcell to examine individual telomeres.

Nanopore analysis, alignment, and telomere length calculation

Base calling to generate FASTQ sequencing files from the electrical signal data (FAST5 files) was performed with GUPPY (v.4.2.3). FASTQ reads containing telomere sequence were selected using TideHunter (v1.4.4) (Gao et al. 2019). Raw base called reads containing the TeloTag were selected using SeqKit (v0.16.1) before alignment (Shen et al. 2016). Nanopore adapters, barcodes, and the TeloTag were removed from reads using Porechop (v0.2.4) before alignment as to not skew length measurement (https://github.com/rrwick/Porechop). FASTQ sequence reads were aligned to a custom reference genome modified from sacCer3 (Foury et al. 1998) (where 2 kb of the *S. cerevisiae* consensus 13-mer telomere repeat sequence [Wahlin and Cohn 2000; Wellinger and Zakian 2012; Li 2018] was added to each chromosome end) using the map-ont preset of minimap2 (v2.18) for alignment of noisy long-read sequences. Custom references for WT W303-0, UE1, UE11, and S288C are available below in GitHub and Supplemental Code. Reads with a map quality score of less than 20, as well as secondary and supplemental reads were filtered out using SAMtools (v1.12), so that only high-confidence alignment primary reads were selected to prevent measuring telomere length of any reads that multimapped to multiple telomeres (Li et al. 2009). The resulting BAM files were examined in the Integrative Genomics Viewer (IGV) (Robinson et al. 2011; Thorvaldsdottir et al. 2013) to ensure that telomere reads are not clipped during alignment, that there are no large indels in the telomere alignment to skew length measurement, and that the telomere alignment begins at the expected "telomere start" position in the reference. BEDTools (v2.30.0) was used to generate files with the start and end chromosomal position of each read from the aligned reads (Quinlan and Hall 2010). These BED files and a BED file with the start position of each telomere end (available for WT W303, UE1, and UE11 references at below) were read into a custom script in RStudio (Supplemental Code; R Core Team 2020) to calculate telomere length for each read and generate plots using the R package ggplot2 (v3.3.3) (Wichman et al. 2016). This R script contains an additional filter to remove any read name duplications within a BED file to again ensure that any multimapping reads are removed. Statistics were calculated using the R package rstatix (v0.7.0) and ANOM (v0.2) (https://cran.r-project.org/web/packages/rstatix/index.html).

Data access

The whole-genome raw sequencing reads data generated in this study have been submitted to the NCBI BioProject database (https://www.ncbi.nlm.nih.gov/bioproject/) under accession number PRJNA730563. The reference genomes, telomere start position files, and code for the above analysis and plots are hosted on GitHub (https://github.com/timplab/Telomere_Length) and are available as Supplemental Code.

Competing interest statement

W.T. has two patents (8,748,091 and 8,394,584) licensed to Oxford Nanopore Technologies.

Acknowledgments

We thank Carla Connelly for strain generation and Southern blotting. We thank Dr. Brendan Cormack, Dr. Rebecca Keener, and Dr. Calla Shubin for thoughtful discussions about experimental design and conclusions. We thank Dr. Rebecca Keener also for assistance in generating analysis scripts. We thank Carla Connelly, Dr. Brendan Cormack, Dr. Rebecca Keener, Dr. Paul Hook, Dr. Akshi Jasani, and Thea Egelhofer for critical reading and editing of the manuscript. This study was supported by the National Institutes of Health, R35CA209974 (to C.W.G.) and U01CA253481 (to W.T.), National Institute of General Medical Sciences, T32 GM007445 (to the BCMB graduate training program), and a Turock Scholar award (to S.L.S.).

References

Abdallah P, Luciano P, Runge KW, Lisby M, Géli V, Gilson E, Teixeira MT. 2009. A two-step model for senescence triggered by a single critically short telomere. *Nat Cell Biol* **11:** 988–993. doi:10.1038/ncb1911

Alexander MK, Zakian VA. 2003. Rap1p telomere association is not required for mitotic stability of a C_3TA_2 telomere in yeast. *EMBO J* **22:** 1688–1696. doi:10.1093/emboj/cdg154

Armanios M. 2013. Telomeres and age-related disease: how telomere biology informs clinical paradigms. *J Clin Invest* **123:** 996–1002. doi:10.1172/JCI66370

Armstrong CA, Tomita K. 2017. Fundamental mechanisms of telomerase action in yeasts and mammals: understanding telomeres and telomerase in cancer cells. *Open Biol* **7:** 160338. doi:10.1098/rsob.160338

Bah A, Gilson E, Wellinger RJ. 2011. Telomerase is required to protect chromosomes with vertebrate-type T2AG3 3′ ends in *Saccharomyces cerevisiae*. *J Biol Chem* **286:** 27132–27138. doi:10.1074/jbc.M111.220186

Berlin K, Koren S, Chin CS, Drake JP, Landolin JM, Phillippy AM. 2015. Assembling large genomes with single-molecule sequencing and locality-sensitive hashing. *Nat Biotechnol* **33:** 623–630. doi:10.1038/nbt.3238

Berthiau AS, Yankulov K, Bah A, Revardel E, Luciano P, Wellinger RJ, Géli V, Gilson E. 2006. Subtelomeric proteins negatively regulate telomere elongation in budding yeast. *EMBO J* **25:** 846–856. doi:10.1038/sj.emboj.7600975

Bianchi A, Shore D. 2008. How telomerase reaches its end: mechanism of telomerase regulation by the telomeric complex. *Mol Cell* **31:** 153–165. doi:10.1016/j.molcel.2008.06.013

Bosco G, Haber JE. 1998. Chromosome break-induced DNA replication leads to non-reciprocal translocations and telomere capture. *Genetics* **150:** 1037–1047. doi:10.1093/genetics/150.3.1037

Brevet V, Berthiau AS, Civitelli L, Donini P, Schramke V, Geli V, Ascenzioni F, Gilson E. 2003. The number of vertebrate repeats can be regulated at yeast telomeres by Rap1-independent mechanisms. *EMBO J* **22:** 1697–1706. doi:10.1093/emboj/cdg155

Chen Q, IJpma A, Greider CW. 2001. Two survivor pathways that allow growth in the absence of telomerase are generated by distinct telomere recombination events. *Mol Cell Biol* **21:** 1819–1827. doi:10.1128/MCB.21.5.1819-1827.2001

Chen H, Xue J, Churikov D, Hass EP, Shi S, Lemon LD, Luciano P, Bertuch AA, Zappulla DC, Géli V, et al. 2018. Structural insights into yeast telomerase recruitment to telomeres. *Cell* **172:** 331–343.e13. doi:10.1016/j.cell.2017.12.008

Claussin C, Chang M. 2016. Multiple Rad52-mediated homology-directed repair mechanisms are required to prevent telomere attrition-induced senescence in *Saccharomyces cerevisiae*. *PLoS Genet* **12:** e1006176. doi:10.1371/journal.pgen.1006176

Counter CM, Avilion AA, LeFeuvre CE, Stewart NG, Greider CW, Harley CB, Bacchetti S. 1992. Telomere shortening associated with chromosome instability is arrested in immortal cells which express telomerase activity. *EMBO J* **11:** 1921–1929. doi:10.1002/j.1460-2075.1992.tb05245.x

Craven RJ, Petes TD. 1999. Dependence of the regulation of telomere length on the type of subtelomeric repeat in the yeast *Saccharomyces cerevisiae*. *Genetics* **152:** 1531–1541. doi:10.1093/genetics/152.4.1531

d'Adda di Fagagna F, Reaper PM, Clay-Farrace L, Fiegler H, Carr P, Von Zglinicki T, Saretzki G, Carter NP, Jackson SP. 2003. A DNA damage checkpoint response in telomere-initiated senescence. *Nature* **426:** 194–198. doi:10.1038/nature02118

Denis E, Sanchez S, Mairey B, Beluche O, Cruaud C, Lemainque A, Wincker P, Barbe V. 2018. Extracting high molecular weight genomic DNA from *Saccharomyces cerevisiae*. Protocol Exchange doi:10.1038/protex.2018.076

Enomoto S, Glowczewski L, Berman J. 2002. *MEC3*, *MEC1*, and *DDC2* are essential components of a telomere checkpoint pathway required for cell cycle arrest during senescence in *Saccharomyces cerevisiae*. *Mol Biol Cell* **13:** 2626–2638. doi:10.1091/mbc.02-02-0012

Feuerhahn S, Iglesias N, Panza A, Porro A, Lingner J. 2010. TERRA biogenesis, turnover and implications for function. *FEBS Lett* **584:** 3812–3818. doi:10.1016/j.febslet.2010.07.032

Foury F, Roganti T, Lecrenier N, Purnelle B. 1998. The complete sequence of the mitochondrial genome of *Saccharomyces cerevisiae*. *FEBS Lett* **440:** 325–331. doi:10.1016/S0014-5793(98)01467-7

Gao Y, Liu B, Wang Y, Xing Y. 2019. TideHunter: efficient and sensitive tandem repeat detection from noisy long-reads using seed-and-chain. *Bioinformatics* **35:** i200–i207. doi:10.1093/bioinformatics/btz376

Gilpatrick T, Lee I, Graham JE, Raimondeau E, Bowen R, Heron A, Downs B, Sukumar S, Sedlazeck FJ, Timp W. 2020. Targeted nanopore sequencing with Cas9-guided adapter ligation. *Nat Biotechnol* **38:** 433–438. doi:10.1038/s41587-020-0407-5

Gilson E, Roberge M, Giraldo R, Rhodes D, Gasser SM. 1993. Distortion of the DNA double helix by RAP1 at silencers and multiple telomeric binding sites. *J Mol Biol* **231:** 293–310. doi:10.1006/jmbi.1993.1283

Gravel S, Larrivée M, Labrecque P, Wellinger RJ. 1998. Yeast Ku as a regulator of chromosomal DNA end structure. *Science* **280:** 741–744. doi:10.1126/science.280.5364.741

Green MR, Sambrook J. 2012. *Molecular cloning: a laboratory manual*, 4th ed. Cold Spring Harbor Laboratory Press, Cold Spring Harbor, NY.

Greider CW. 1996. Telomere length regulation. *Annu Rev Biochem* **65:** 337–365. doi:10.1146/annurev.bi.65.070196.002005

Greider CW. 1998. Telomerase activity, cell proliferation, and cancer. *Proc Natl Acad Sci* **95:** 90–92. doi:10.1073/pnas.95.1.90

Greider CW. 2016. Regulating telomere length from the inside out: the replication fork model. *Genes Dev* **30:** 1483–1491. doi:10.1101/gad.280578.116

Greider CW, Blackburn EH. 1985. Identification of a specific telomere terminal transferase activity in *Tetrahymena* extracts. *Cell* **43:** 405–413. doi:10.1016/0092-8674(85)90170-9

Grigorev K, Foox J, Bezdan D, Butler D, Luxton JJ, Reed J, McKenna MJ, Taylor L, George KA, Meydan C, et al. 2021. Haplotype diversity and sequence heterogeneity of human telomeres. *Genome Res* doi:10.1101/gr.274639.120

Hardy CF, Sussel L, Shore D. 1992. A RAP1-interacting protein involved in transcriptional silencing and telomere length regulation. *Genes Dev* **6:** 801–814. doi:10.1101/gad.6.5.801

Henning KA, Moskowitz N, Ashlock MA, Liu PP. 1998. Humanizing the yeast telomerase template. *Proc Natl Acad Sci* **95:** 5667–5671. doi:10.1073/pnas.95.10.5667

IJpma A, Greider CW. 2003. Short telomeres induce a DNA damage response in *Saccharomyces cerevisiae*. *Mol Biol Cell* **14:** 987–1001. doi:10.1091/mbc.02-04-0057

Kaizer H, Connelly CJ, Bettridge K, Viggiani C, Greider CW. 2015. Regulation of telomere length requires a conserved N-terminal domain of Rif2 in *Saccharomyces cerevisiae*. *Genetics* **201:** 573–586. doi:10.1534/genetics.115.177899

Keener R, Connelly CJ, Greider CW. 2019. Tel1 activation by the MRX complex is sufficient for telomere length regulation but not for the DNA damage response in *Saccharomyces cerevisiae*. *Genetics* **213:** 1271–1288. doi:10.1534/genetics.119.302713

Kovaka S, Fan Y, Ni B, Timp W, Schatz MC. 2021. Targeted nanopore sequencing by real-time mapping of raw electrical signal with UNCALLED. *Nat Biotechnol* **39:** 431–441. doi:10.1038/s41587-020-0731-9

Laterreur N, Lemieux B, Neumann H, Berger-Dancause JC, Lafontaine D, Wellinger RJ. 2018. The yeast telomerase module for telomere

recruitment requires a specific RNA architecture. *RNA* **24:** 1067–1079. doi:10.1261/rna.066696.118
Lebel C, Rosonina E, Sealey DC, Pryde F, Lydall D, Maringele L, Harrington LA. 2009. Telomere maintenance and survival in *Saccharomyces cerevisiae* in the absence of telomerase and *RAD52*. *Genetics* **182:** 671–684. doi:10.1534/genetics.109.102939
Lendvay TS, Morris DK, Sah J, Balasubramanian B, Lundblad V. 1996. Senescence mutants of *Saccharomyces cerevisiae* with a defect in telomere replication identify three additional *EST* genes. *Genetics* **144:** 1399–1412. doi:10.1093/genetics/144.4.1399
Li H. 2018. Minimap2: pairwise alignment for nucleotide sequences. *Bioinformatics* **34:** 3094–3100. doi:10.1093/bioinformatics/bty191
Li H, Handsaker B, Wysoker A, Fennell T, Ruan J, Homer N, Marth G, Abecasis G, Durbin R, 1000 Genome Project Data Processing Subgroup. 2009. The Sequence Alignment/Map format and SAMtools. *Bioinformatics* **25:** 2078–2079. doi:10.1093/bioinformatics/btp352
Louis EJ, Haber JE. 1990. Mitotic recombination among subtelomeric Y′ repeats in *Saccharomyces cerevisiae*. *Genetics* **124:** 547–559. doi:10.1093/genetics/124.3.547
Louis EJ, Haber JE. 1992. The structure and evolution of subtelomeric Y′ repeats in *Saccharomyces cerevisiae*. *Genetics* **131:** 559–574. doi:10.1093/genetics/131.3.559
Lundblad V, Blackburn EH. 1993. An alternative pathway for yeast telomere maintenance rescues *est1*$^{-}$ senescence. *Cell* **73:** 347–360. doi:10.1016/0092-8674(93)90234-H
Lundblad V, Szostak JW. 1989. A mutant with a defect in telomere elongation leads to senescence in yeast. *Cell* **57:** 633–643. doi:10.1016/0092-8674(89)90132-3
Lyčka M, Peska V, Demko M, Spyroglou I, Kilar A, Fajkus J, Fojtová M. 2021. WALTER: an easy way to online evaluate telomere lengths from terminal restriction fragment analysis. *BMC Bioinformatics* **22:** 145. doi:10.1186/s12859-021-04064-0
Maciejowski J, de Lange T. 2017. Telomeres in cancer: tumour suppression and genome instability. *Nat Rev Mol Cell Biol* **18:** 175–186. doi:10.1038/nrm.2016.171
Marcand S, Gilson E, Shore D. 1997. A protein-counting mechanism for telomere length regulation in yeast. *Science* **275:** 986–990. doi:10.1126/science.275.5302.986
Marcand S, Brevet V, Gilson E. 1999. Progressive *cis*-inhibition of telomerase upon telomere elongation. *EMBO J* **18:** 3509–3519. doi:10.1093/emboj/18.12.3509
Matheson K, Parsons L, Gammie A. 2017. Whole-genome sequence and variant analysis of W303, a widely-used strain of *Saccharomyces cerevisiae*. *G3 (Bethesda)* **7:** 2219–2226. doi:10.1534/g3.117.040022
Maxwell PH, Coombes C, Kenny AE, Lawler JF, Boeke JD, Curcio MJ. 2004. Ty1 mobilizes subtelomeric Y′ elements in telomerase-negative *Saccharomyces cerevisiae* survivors. *Mol Cell Biol* **24:** 9887–9898. doi:10.1128/MCB.24.22.9887-9898.2004
McEachern MJ, Haber JE. 2006. Break-induced replication and recombinational telomere elongation in yeast. *Annu Rev Biochem* **75:** 111–135. doi:10.1146/annurev.biochem.74.082803.133234
McNally EJ, Luncsford PJ, Armanios M. 2019. Long telomeres and cancer risk: the price of cellular immortality. *J Clin Invest* **129:** 3474–3481. doi:10.1172/JCI120851
Moyzis RK, Buckingham JM, Cram LS, Dani M, Deaven LL, Jones MD, Meyne J, Ratliff RL, Wu J-R. 1988. A highly conserved repetitive DNA sequence, (TTAGGG)n, present at the telomeres of human chromosomes. *Proc Natl Acad Sci* **85:** 6622–6626. doi:10.1073/pnas.85.18.6622
Noma KI. 2017. The yeast genomes in three dimensions: mechanisms and functions. *Annu Rev Genet* **51:** 23–44. doi:10.1146/annurev-genet-120116-023438
Pallmann J, Hothorn LA. 2016. Analysis of means: a generalized approach using R. *J Appl Stat* **43:** 1541–1560. doi:10.1080/02664763.2015.1117584
Paschini M, Reyes CM, Gillespie AE, Lewis KA, Glustrom LW, Sharpee TO, Wuttke DS, Lundblad V. 2020. Spontaneous replication fork collapse regulates telomere length homeostasis in wild type cells. bioRxiv doi:10.1101/2020.08.05.237172
Quinlan AR, Hall IM. 2010. BEDTools: a flexible suite of utilities for comparing genomic features. *Bioinformatics* **26:** 841–842. doi:10.1093/bioinformatics/btq033
R Core Team. 2020. *R: a language and environment for statistical computing*. R Foundation for Statistical Computing, Vienna. https://www.R-project.org/.
Robinson JT, Thorvaldsdóttir H, Winckler W, Guttman M, Lander ES, Getz G, Mesirov JP. 2011. Integrative genomics viewer. *Nat Biotechnol* **29:** 24–26. doi:10.1038/nbt.1754
Shampay J, Blackburn EH. 1988. Generation of telomere-length heterogeneity in *Saccharomyces cerevisiae*. *Proc Nat Acad Sci* **85:** 534–538. doi:10.1073/pnas.85.2.534
Shen W, Le S, Li Y, Hu F. 2016. SeqKit: a cross-platform and ultrafast toolkit for FASTA/Q file manipulation. *PLoS One* **11:** e0163962. doi:10.1371/journal.pone.0163962
Shubin CB, Mayangsari R, Swett AD, Greider CW. 2021. Rif1 regulates telomere length through conserved HEAT repeats. *Nucleic Acids Res* **49:** 3967–3980. doi:10.1093/nar/gkab206
Smogorzewska A, de Lange T. 2004. Regulation of telomerase by telomeric proteins. *Annu Rev Biochem* **73:** 177–208. doi:10.1146/annurev.biochem.73.071403.160049
Sobecki M, Souaid C, Boulay J, Guerineau V, Noordermeer D, Crabbe L. 2018. MadID, a versatile approach to map protein-DNA interactions, highlights telomere-nuclear envelope contact sites in human cells. *Cell Rep* **25:** 2891–2903.e5. doi:10.1016/j.celrep.2018.11.027
Stanley SE, Armanios M. 2015. The short and long telomere syndromes: paired paradigms for molecular medicine. *Curr Opin Genet Dev* **33:** 1–9. doi:10.1016/j.gde.2015.06.004
Teixeira MT, Arneric M, Sperisen P, Lingner J. 2004. Telomere length homeostasis is achieved via a switch between telomerase- extendible and -nonextendible states. *Cell* **117:** 323–335. doi:10.1016/S0092-8674(04)00334-4
Teng SC, Zakian VA. 1999. Telomere-telomere recombination is an efficient bypass pathway for telomere maintenance in *Saccharomyces cerevisiae*. *Mol Cell Biol* **19:** 8083–8093. doi:10.1128/MCB.19.12.8083
Thorvaldsdottir H, Robinson JT, Mesirov JP. 2013. Integrative Genomics Viewer (IGV): high-performance genomics data visualization and exploration. *Brief Bioinform* **14:** 178–192. doi:10.1093/bib/bbs017
Wahlin J, Cohn M. 2000. *Saccharomyces cerevisiae* RAP1 binds to telomeric sequences with spatial flexibility. *Nucleic Acids Res* **28:** 2292–2301. doi:10.1093/nar/28.12.2292
Watson JM, Riha K. 2010. Comparative biology of telomeres: where plants stand. *FEBS Lett* **584:** 3752–3759. doi:10.1016/j.febslet.2010.06.017
Wellinger RJ, Zakian VA. 2012. Everything you ever wanted to know about *Saccharomyces cerevisiae* telomeres: beginning to end. *Genetics* **191:** 1073–1105. doi:10.1534/genetics.111.137851
Wichman H, Navarro D, Pendersen TL. 2016. *ggplot2: elegant graphics for data analysis*. Springer, New York.
Xu Z, Duc KD, Holcman D, Teixeira MT. 2013. The length of the shortest telomere as the major determinant of the onset of replicative senescence. *Genetics* **194:** 847–857. doi:10.1534/genetics.113.152322

Received June 6, 2021; accepted in revised form October 20, 2021.